Development at the University of North Dakota of a Digital Thermosonde Instrument for the Study of Atmospheric Optical Turbulence (C_n^2)

Blake Sorenson[*a], James Casler[b], and David Delene[a]*

[a]*Department of Atmospheric Sciences, University of North Dakota, Grand Forks, ND*
[b]*Department of Space Studies, University of North Dakota, Grand Forks, ND*

*Students: blake.sorenson@und.edu**
Mentor: james.casler@und.edu david.delene@und.edu

ABSTRACT

Atmospheric optical turbulence affects the transmission of electromagnetic waves between the Earth's surface and orbit. High optical turbulence results in noisier ground to satellite communication and degraded satellite images. Earth surface images obtained from satellites, and stellar object images from ground telescopes, are enhanced greatly when accounting for optical turbulence in real time. To study optical turbulence profiles, a NASA Undergraduate Student Instrument Project (USIP) at the University of North Dakota (UND) constructed a balloon-borne, digital thermosonde that measures high-resolution temperature differences using a fine-wire platinum thermocouple. The USIP team used a design based on work done by NASA in the 1970s and improved on by the Air Force Research Laboratory (AFGL). Two tethered balloon flights indicate that the thermosonde measured temperature difference agrees with the low-end of the expected temperature differences derived from National Weather Service sounding data. Two free flying balloon flights measured refractive index structure parameter profiles similar to those obtained from Graw radiosondes. The thermosonde horizontal temperature differences are similar to the vertical temperature differences measured by the radiosonde. The differences between the refractive index structure parameter profiles obtained using the thermocouple and the radiosonde are consistent with previous studies. The USIP team demonstrated that undergraduate students can successfully build a thermosonde system based on the NASA/AFGL design and deploy the thermosonde system to obtain optical turbulence measurements.

KEYWORDS

Optical turbulence; refractive index structure parameter; thermosonde; radiosonde; ballooning; airborne measurements; vertical profile

INTRODUCTION

Temperature differences, particulate matter, and precipitation distort wireless communications through the Earth's atmosphere.[1] Differences in atmospheric temperature affect the transmission of electromagnetic signals, including visible light. Just as light passing from air into water causes images of underwater objects to appear distorted, atmospheric layers of different density bend light differently causing distortions. Larger differences in layer density result in higher image distortion and increased noise for communication signals. For laser systems, density variations cause beam steering, image dancing, and beam spreading, which affect image and communication quality.[2] Atmospheric optical turbulence is defined as the distortion of light passing through the atmosphere caused by layers with differing density. Density differences cause optical turbulence mainly due to temperature and humidity variations. Temperature variations are important throughout the troposphere, while humidity variations are primarily important in the planetary boundary layer since water vapor content above the planetary boundary layer is typically low and thus has little effect on density variations.

Optical turbulence research dates back to the early 1960s when Tatarski first proposed a relationship between density and turbulence.[3] Optical turbulence is usually quantified by the refractive index structure parameter, C_n^2, and can be calculated using Obukhov-Kolmogorov turbulence theory, which has the temperature structure parameter given by

$$C_T{}^2(h) = \left\{\frac{[T(d_1) - T(d_2)]^2}{d^{\frac{2}{3}}}\right\}, \qquad \textbf{Equation 1.}$$

where $\mathrm{T(d_1)}$ and $\mathrm{T(d_2)}$ are high-resolution horizontal temperature measurements and $d = |d_2 - d_1|$ is the distance between two temperature measurements.[4, 5] C_n^2 is related to C_T^2 by standard meteorological parameters using the Dale-Gladstone Relationship,

$$C_n^2 = (79 * 10^{-6}(\frac{P}{T^2}))^2 C_T^2, \quad \textbf{Equation 2.}$$

where P is atmospheric pressure in mb and T is temperature in Kelvin.[3]

The thermosonde, an instrument that measures temperature differences, was developed in the late 1960s and early 1970s. The thermosonde uses two 2 μm diameter platinum wires spaced one meter apart to measure temperature difference.[6] The first balloon-borne temperature difference profiles showed that areas of high optical turbulence are confined to the surface boundary layer, the lower troposphere, and the tropopause. The layers corresponded to areas of high wind shear and temperature inversions.

The refractive index structure parameter can be determined using temperature differences from atmospheric models. The Air Force Geophysical Lab (now the Air Force Research Laboratory) developed the Dewan model, which has become one of the more widely used models for calculating the refractive index structure parameter. The Dewan (AFGL) model defines optical turbulence using:

$$C_n^2 = 2.8[(\frac{79 \times 10^{-6} P}{T^2})(\frac{\partial T}{\partial z} + \gamma)]^2 (0.1)^{4/3} 10^{Y(z)}, \quad \textbf{Equation 3.}$$

where

$$Y(z) = 1.64 + 42.0 \times S_{raw} \textbf{ (Troposphere)} \quad \textbf{Equation 4.}$$

$$Y(z) = 0.506 + 50.0 \times S_{raw} \textbf{ (Stratosphere)} \quad \textbf{Equation 5.}$$

and

$$S_{\mathrm{raw}} = \sqrt{\frac{\partial \mathrm{u}^2}{\partial \mathrm{z}} + \frac{\partial \mathrm{v}^2}{\partial \mathrm{z}}} \quad \textbf{Equation 6.}$$

where P is atmospheric pressure in mb, T is temperature in Kelvin, γ is the dry adiabatic lapse rate, u is the zonal wind component, and v is the meridional wind component.[7] Other optical turbulence-estimating models have been developed to estimate the refractive index structure parameter from standard meteorological profile data, including the Hufnagel and Van Zandt models,[8, 9] but a comparison study indicated that between the Hufnagel, Van Zandt, and AFGL models, the AFGL model outperformed the others at estimating the refractive index structure parameter.[7] Due to the complexity of modeling boundary layer turbulence, the AFGL model is not valid for the boundary layer. The AFGL model does not account for moisture-induced density fluctuations; therefore, the model is more suitable for the drier atmosphere above the boundary layer.[7] Hence, only measurements above 3 km (maximum boundary layer height) are analyzed using the AFGL model. A thermosonde measurement of C_n^2 has been compared to the high-resolution Weather Research and Forecasting (WRF) model, with logarithmic differences between the radiosonde-estimated C_n^2 and the WRF forecasts of ${C_n}^2$ found to be 0.090 ± 0.823.[11] A potential source of error with using the platinum-wire thermosonde is the impact of solar heating. Richardson found that solar heating of the 4.7 μm diameter platinum-coated tungsten wires could cause errors of two orders of magnitude on C_n^2 measurements.[10] To reduce the impact of solar heating, thinner wires made of more reflective and thermally-smooth metals such as pure platinum, silver, or aluminum can be used.[10]

METHODS

The digital thermosonde is based on the Air Force Research Laboratory designs from the 1970s, which has been used in various projects over the last 50 years.[6, 12] The thermosonde measures temperature difference using two 2 μm diameter platinum wire probes (**Figure 1**). The temperature probe is two arms of an unbalanced Wheatstone Bridge that provides the 1 m temperature difference measurement as a voltage difference. The voltage difference is amplified, conditioned, and converted to an analog signal representing the root mean square of the voltage difference, which is measured by a high precision analog-to-digital board and stored locally on a Secure Digital (SD) card and sent to the ground using the XDATA protocol of the Graw radiosonde. XDATA is a standard protocol for chaining together data from multiple instruments into the radiosonde's data stream.[13] Graw DFM-09 radiosondes (white probe in **Figure 1**) measures the standard meteorological parameters of pressure, temperature, wind, and altitude. The radiosonde sends data to a ground receiving station at 24 bps.

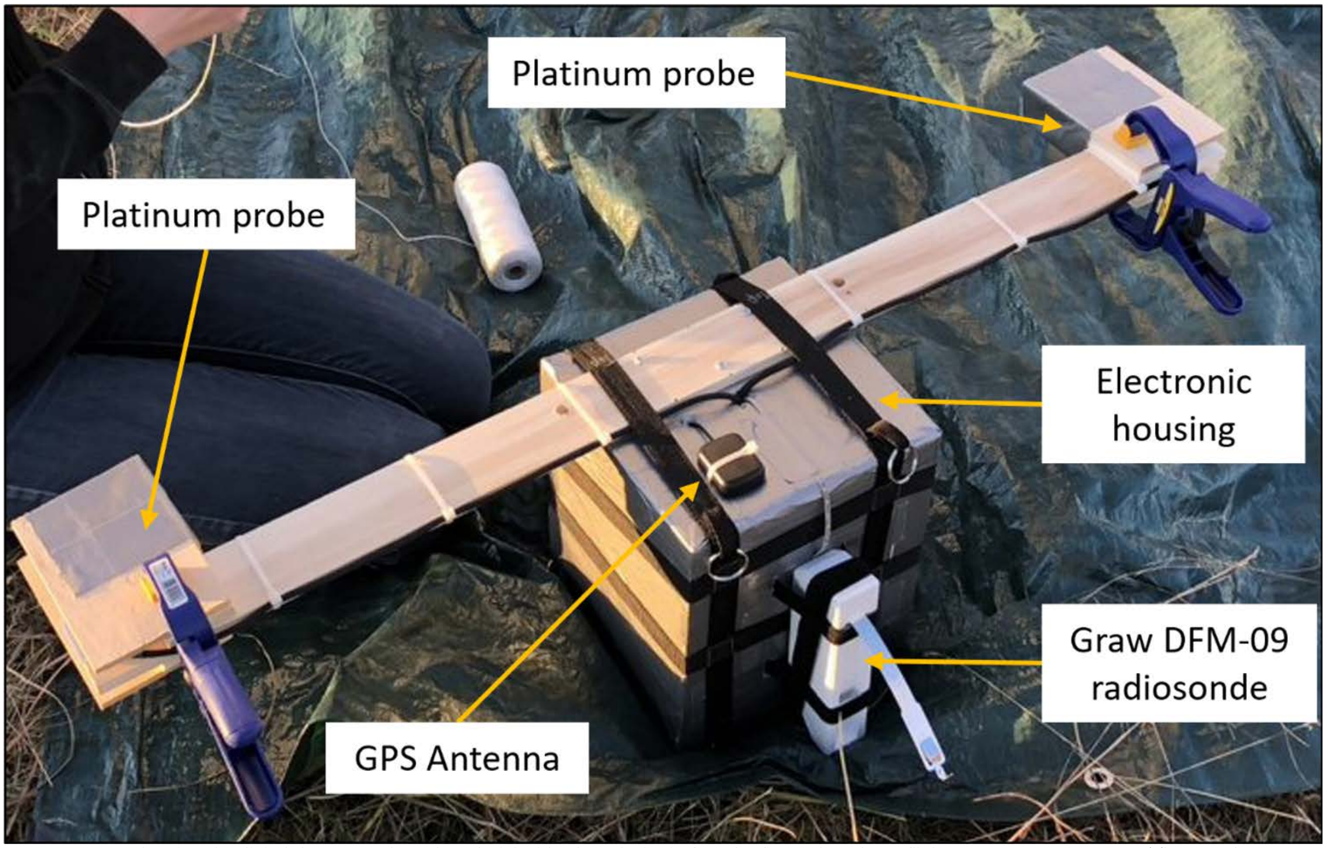

Figure 1. Image showing the digital thermosonde at the Glacial Ridge launch site before the first tethered test flight on 29 September 2017. The grey duct tape-covered box in the center contains the thermosonde electrical components, the Raspberry Pi, and a GPS receiver. A 1 m long wooden board is secured along the Styrofoam box with two daughter boards at the board ends that contain the 2 μm diameter platinum wire probes. A shield made from two wood blocks is secured around the probes until launch to prevent probe damage during balloon systems preparation.

The thermosonde is part of a balloon package system (**Figure 2**) that records voltage difference throughout a typical 2.5 hr flight, which includes both balloon ascent and descent after balloon burst. To minimize thermal wake effects caused by the balloon's ascent, the thermosonde is suspended in a harness 55 meters below the balloon.[14] The Raspberry Pi inside the thermosonde sends voltage difference data to the radiosonde, which transmits the data to the ground station along with radiosonde data. The ground station uses a Graw omnidirectional antenna mounted vertically a few feet above ground level to receive the data using a laptop and the Grawmet sounding software. The voltage difference measurements are stored in raw data files (.gsf file extension), while the radiosonde measurements are saved as text files.

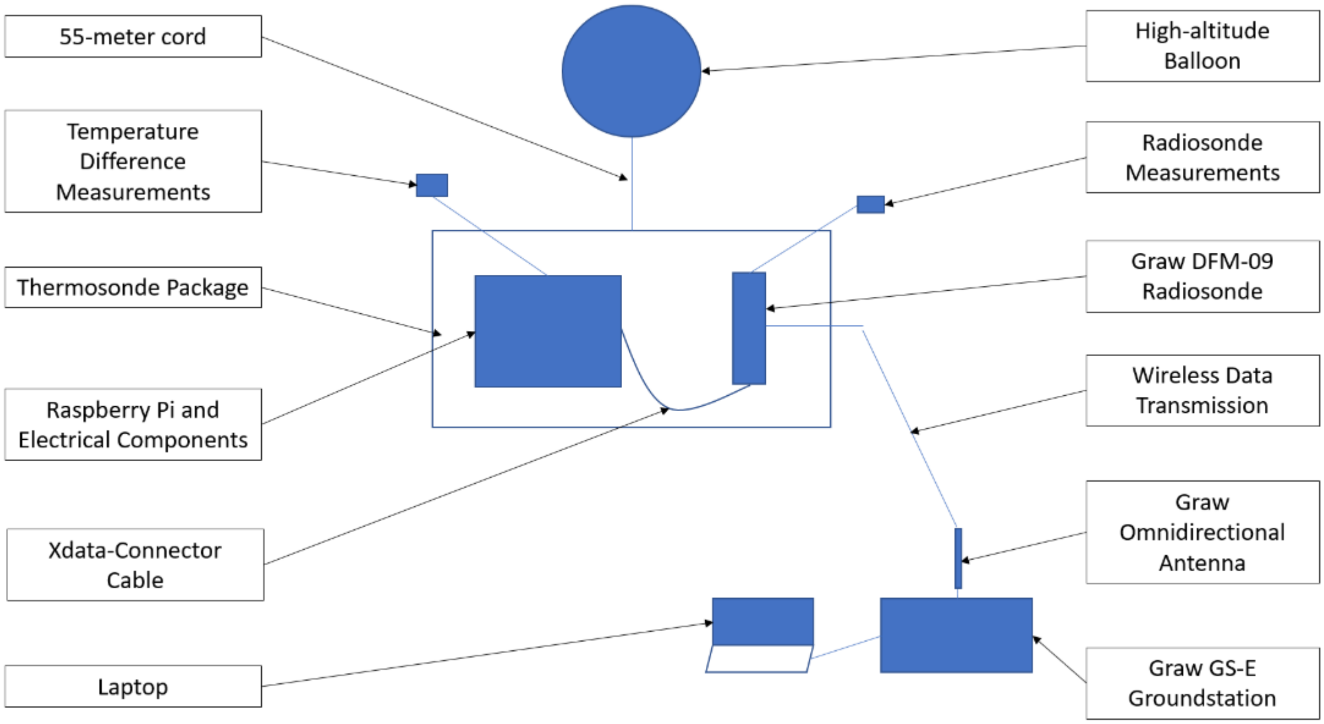

Figure 2. Block diagram (not to scale) showing the balloon package components and the data transferred through the system. The Thermosonde voltage difference measurement is sent from the Raspberry Pi to the Graw radiosonde (DFM-09) using the radiosonde's XDATA cable. The voltage difference data are transmitted to the ground station along with radiosonde data.

The thermosonde voltage representing the temperature difference includes noise that results in an approximately 0.23 V offset. The voltage offset must be addressed to ensure the voltage represents a true temperature difference. To determine the voltage offset, data from a 11 November 2017 test flight are analyzed, in which the thermosonde is attached to a tether balloon system and flown to approximately 500 ft above ground level. The test flight data are used to correct the thermosonde's voltage measurements by determining relationships between the raw voltage measurements and the corrected voltages. For root mean square voltages less than 0.66 V, the relation between the raw and corrected voltages (**Figure 3a**) is logarithmic, while the relationship is linear for voltages larger than 0.66 V. These relations are given by the following equations,

$$V_{corrected} = 0.553 * ln(V_{rms}) + 0.844 \text{ , } for\ V_{rms} \leq 0.66\ V \qquad \textbf{Equation 7.}$$

$$V_{corrected} = 1.019 * V_{rms} - 0.048 \qquad , for\ V_{rms} > 0.66\ V \qquad \textbf{Equation 8.}$$

where V_{rms} is the raw root mean square (RMS) voltage measured by the thermosonde, with the root mean square voltage being the square root of the mean square of the instantaneous voltage values sampled by the sensor. The RMS voltage can also be described as the amount of alternating current (AC) power drawn from a resistor similar to the power drawn by a direct current (DC). The corrected voltages are converted to temperature difference using a linear equation given by,

$$\Delta T = 0.129 V_{corrected} \qquad \textbf{Equation 9.}$$

where $V_{corrected}$ is the thermosonde voltage calculated with the calibration equations given by **Equation 7** and **Equation 8**. Unlike the voltage relationship, which is logarithmic for smaller voltages and linear for larger voltages, the relation between the corrected voltage and temperature differences (**Figure 3b**) is linear for all voltages.

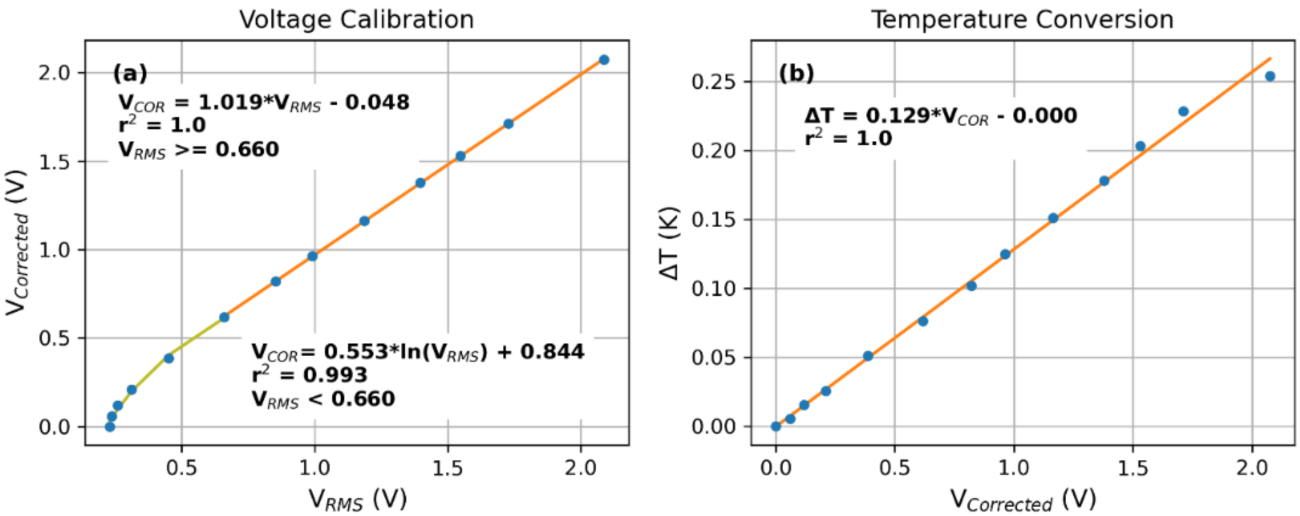

Figure 3. (a, left) The relationship) between the root mean square voltage (V_{rms}) measured by the thermosonde and the corrected voltage ($V_{corrected}$) using data from the Glacial Ridge field site on 17 November 2017. (b, right) The relation between the corrected voltage ($V_{corrected}$) on the thermosonde's Wheatstone bridge and the temperature difference measured by the platinum-wire probes (ΔT).

In addition to the measured thermosonde $C_n{}^2$ profiles and estimated profiles from the radiosonde data, additional estimates of $C_n{}^2$ are obtained from High-resolution Rapid Refresh (HRRR) model data. The HRRR model sounding data are obtained from the NOAA Air Resources Laboratory (ARL) Archived Meteorology database (https://www.ready.noaa.gov/READYamet.php), and each profile is retrieved for the latitude and longitude of the thermosonde launch site. The HRRR soundings have 3 km horizontal grid spacing and roughly 50 vertical levels. The radiosonde and thermosonde profiles have much higher vertical resolution than the HRRR profile, so the radiosonde and thermosonde data are averaged to match the vertical resolution of the model profile for comparison. All data from a thermosonde launch are processed to extract voltage measurements from the xml-formatted Graw files. Profiles of the refractive index structure parameter are calculated for the thermosonde, radiosonde and model data. All programs used for data analysis are part of the open-source Airborne Data Processing and Analysis (ADPAA) software package.[15]

To collect measurements for calculating the refractive index structure parameter, the thermosonde system was launched from the UND Glacial Ridge Atmospheric Observatory southeast of Crookston, Minnesota and from Mayville State University in Mayville, North Dakota. The long (55 m) suspension line for the thermosonde creates issues that are not present during a balloon launch in which the package is located close to the balloon. Even an experienced launch team needs to understand and review these differences to ensure a safe and successful launch. Enough area is required to lay out the line between the balloon and package. The balloon needs to lift the package high enough to clear any obstructions around the launch site. The main obstructions at the Glacial Ridge site are power lines on the west side of the site and a fence around the trailer and wind profiler (**Figure 4**). The 5 May 2018 launch had an easterly wind; therefore, the balloon is positioned on the east side and the line strung out to the west so the balloon rises above the line when released. Depending on the wind speed, those holding the line and package need to move towards the balloon to allow the line and package to be lifted straight up out of their hands. Having the line and package lifted straight up ensures that it is not dragged along the ground and damaged. Additionally, there needs to be enough "Clearance Distance" to ensure that the package does not hit any obstructions. The power line obstruction is 10.4 m (34 ft) above ground and the maximum allowed wind speed for a launch is 6.7 m/s (15 mile per hour); therefore, a "Clearance Distance" of 25.7 m (or 3.84 s) is required, assuming a 2.7 m/s (530 ft/min) ascent rate. Hence, the balloon needs to be a total of 80.7 m (25.7 + 55 m) from the power line for an easterly wind. A tarp is useful for laying out the suspension line and an anchor helps so people do not have to hold the balloon when attaching the thermosonde package. It can be difficult to hold the balloon on a cold night, especially if there is a delay in getting the thermosonde package ready. Sufficient helium is added to the balloon to have a rate of approximately 5 m s^{-1}. With the thermosonde's 5 Hz data sampling rate, the vertical resolution is 1 m.

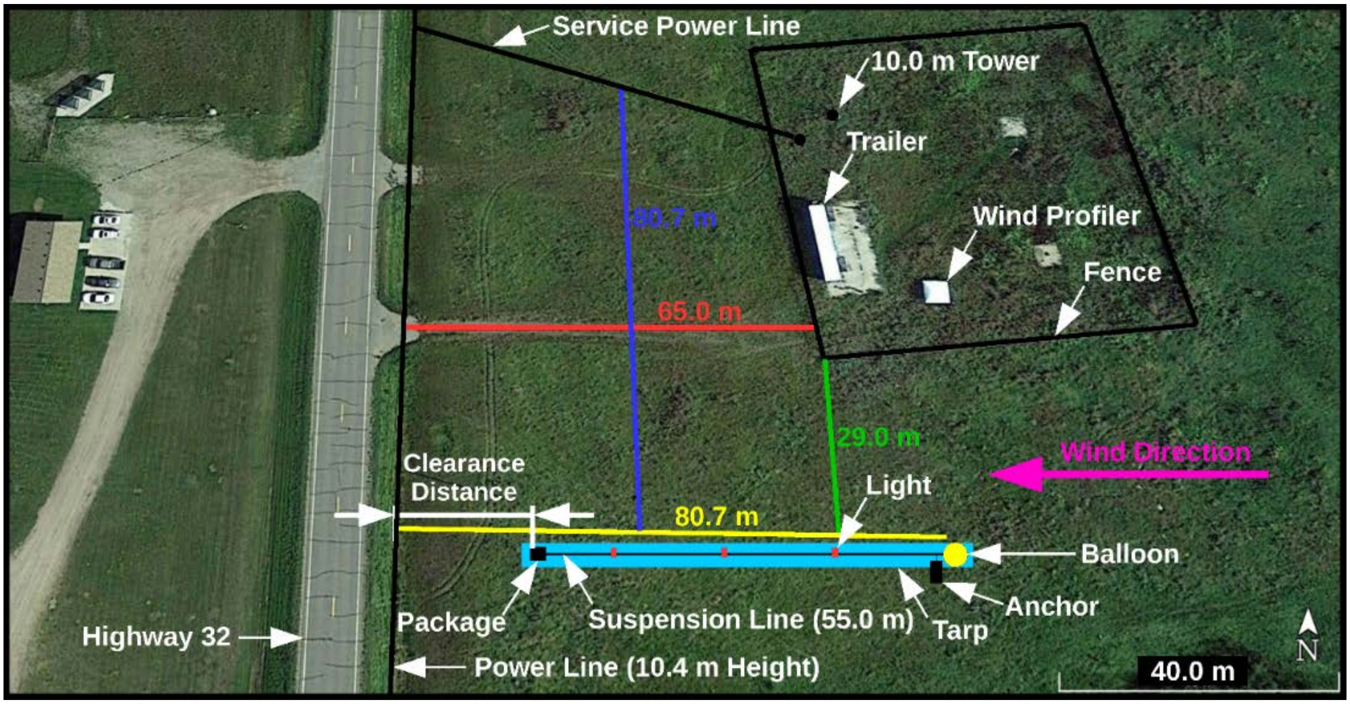

Figure 4. Google Earth image showing the University of North Dakota Glacial Ridge Atmospheric Observatory (GRAO) field site with labels depicting the lay out for a balloon launch with an easterly wind.

RESULTS

A) Synthetic Testing Data Set

To determine the expected range of thermosonde measurements, a synthetic testing data set is generated using climatological temperature difference profiles generated from all 00 UTC Bismarck radiosonde profiles obtained during November of 2017. The data set (Appendix A) consists of the average and standard deviation of NWS radiosonde-estimated C_n^2 from the surface to 10 mb. In the 00Z November 2017 climatology of estimated C_n^2 (**Figure 5**), the most variability in C_n^2 is from the surface to 925 mb, which is expected due to the high variability of temperature and wind near the surface. The median C_n^2 value increases slightly and the range decreases significantly in the 925-850 mb layer. The median values decrease from 850 mb to 300 mb. The 300 - 200 mb layer C_n^2 is higher than in the layers above and below, likely associated with the temperature inversion and high static stability associated with the tropopause. Above 200 mb, the C_n^2 values decrease.

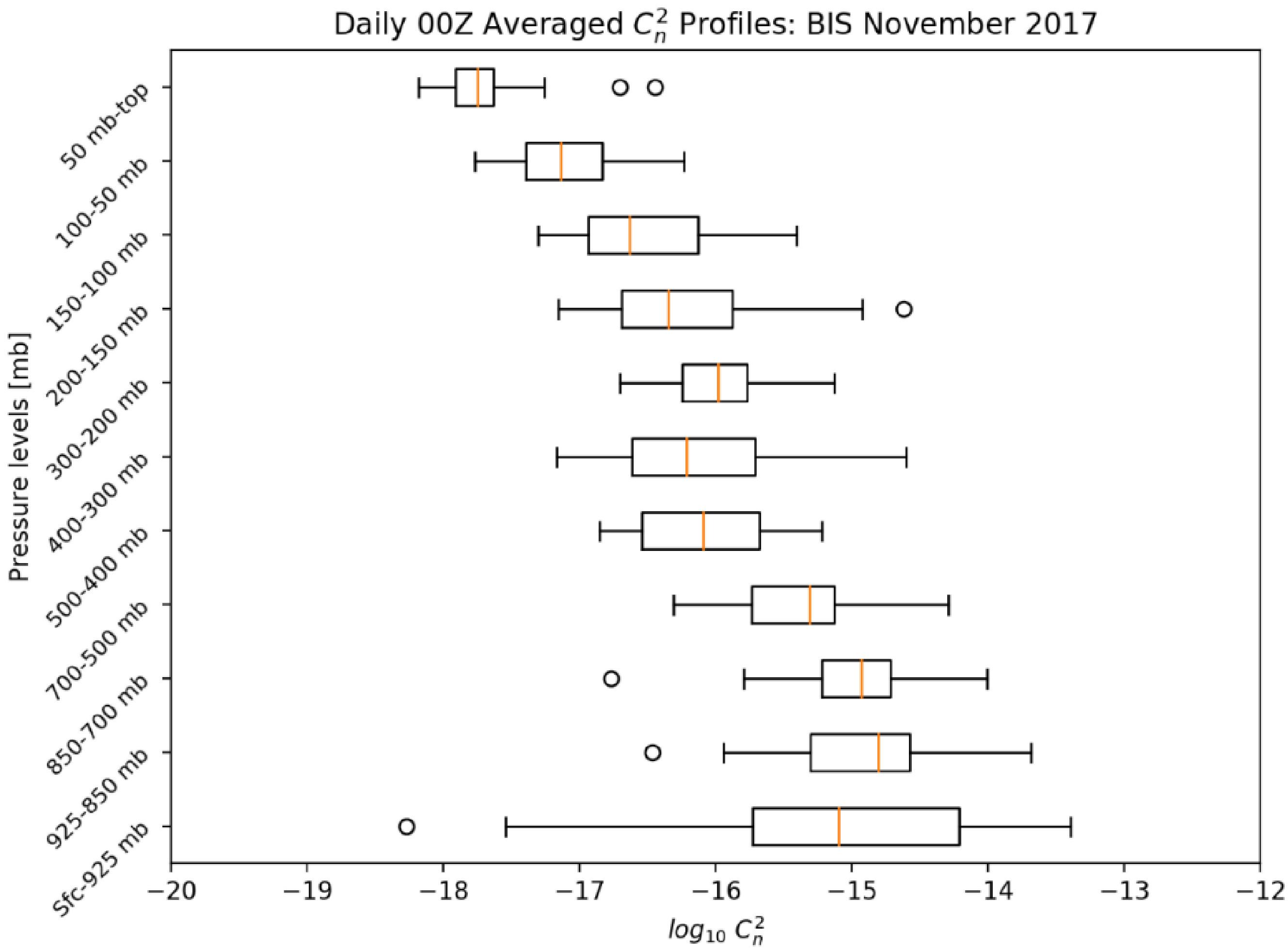

Figure 5. Box-and-whisker plot showing the estimated Bismarck C_n^2 climatology for 00Z November 2017, with the C_n^2 calculated using the Dewan method. Each layer has its own box-and-whisker to represent the range of C_n^2, with the orange lines in the center of each boxplot representing the median logarithmic C_n^2 in the layer. The ends of the boxes denote the interquartile range (from the lowest 25% of the data to the highest 75%), and the circles in the boxplots indicate outliers.

To generate a testing data set from the November 2017 monthly climatology, a random number generator is used to obtain random structure parameters within one standard deviation of the mean. A synthetic dataset consisting of expected C_n^2 in each layer of the atmosphere is created for comparison to the thermosonde measurements. The synthetic C_n^2 is determined using temperatures between each layer in the monthly climatology, using equations:

$$C_{n\,i,j}^2 = \overline{C_n^2}_{i,j} + \sigma_{C_{n\,i}^2}(2R-1) \quad \textbf{Equation 10.}$$

$$T_{i,j} = \bar{T}_{i,j} + \sigma_{T\,i}(2R-1) \quad \textbf{Equation 11.}$$

where *i* indicates an individual climatology level (i.e. 925 mb – 850 mb), *j* indicates a specific height within the *i* level for which synthetic data are calculated, $C_{n\,i,j}^2$ and $T_{i,j}$ are the synthetic refractive index structure parameter and temperatures, respectively. $\overline{C_n^2}_{i,j}$ and $\bar{T}_{i,j}$ are the base refractive index structure parameter and temperatures interpolated between the i and i+1 level climatology averages, $\sigma_{C_{n\,i}^2}$ and $\sigma_{T\,i}$ are the standard deviations of the refractive index structure parameter and temperature climatologies for the current level and R is a random value between 0 and 1.

While the synthetic dataset (**Figure 6a**) provides the C_n^2 range in each atmospheric layer, a C_n^2 profile that more smoothly matches the layers directly above and below is more desired for testing purposes. Synthetic temperature difference data are calculated from synthetic C_n^2 by reversing the Dale-Gladstone equation (Equation 2) and solving for C_T^2 in terms of pressure, temperature, and C_n^2.

Upon reversing Equation 2 and inserting Equation 1 to get the temperature difference from C_T^2, the synthetic temperature difference equation is:

$$\Delta T_s = \sqrt{\frac{C_{n_s}^2 * d^{2/3}}{(79 * 10^{-6}(\frac{P}{T^2}))^2}}$$ **Equation 12.**

where d is the distance between the two platinum wire probes (1 meter), P is the atmospheric pressure in mb, and T is the temperature in Kelvin. The temperature difference testing dataset, shown in **Figure 6b**, is used to determine if the temperature difference measurements from a balloon flight are within an expected range. The temperature difference in the upper atmosphere (> 20 km) increases with height because the reversed Dale-Gladstone relation (Equation 12) contains a squared pressure in the denominator. Hence, as pressure decreases linearly, the synthetic temperature difference increases exponentially.

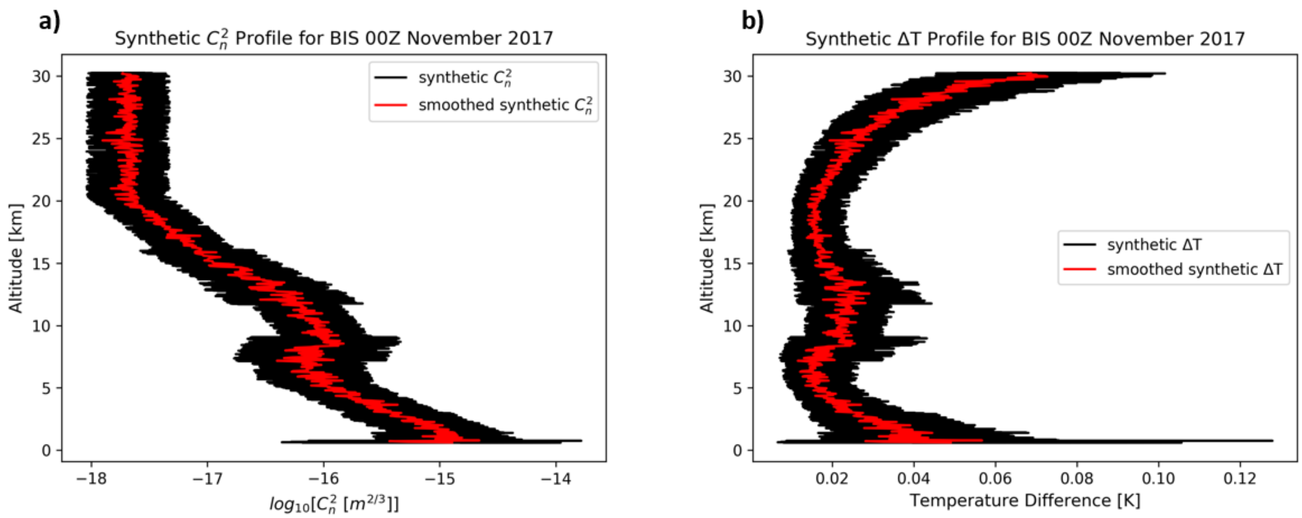

Figure 6. Plots showing the synthetic refractive index structure parameter ($C_{n_s}^2$) **(a)** and synthetic temperature difference (ΔT_s) **(b)** datasets calculated with the 00Z November 2017 Bismarck sounding climatology. The black line is the raw $C_{n_s}^2/\Delta T_s$ for every 5 m from the surface to 30 km. The red line is a 11-point running average of $C_{n_s}^2/\Delta T_s$.

B) 5 May 2018 Balloon Flight

A night balloon launch was conducted starting 4 May and ending 5 May 2018. Compared to daytime, a night profile has reduced thermal turbulence caused by the balloon.[11] During the day, the latex balloon is warmed by the sun, and as the balloon ascends, air contacts the balloon and warms. The warmed air is pulled into the balloon's turbulent wake causing additional turbulence below the balloon. Suspending the thermosonde 50 m below the balloon minimizes the balloon's wake effect. The thermosonde ascends at 5 m s^{-1} to an altitude of 28 km where the balloon bursts and the package descends to the surface.

After analyzing the time series of the raw thermosonde voltages from the free-flight launch, an instrument noise floor of 0.2 V is chosen for the free flight. The raw voltages are corrected to account for the instrument noise floor using the equations:

$$V_{corrected} = 0.4696 * ln(V_{rms}) + 0.7847\ , for\ V_{rms} \leq 0.436\ V$$ **Equation 13.**

$$V_{corrected} = 1.0206 * V_{rms} - 0.046 \qquad , for\ V_{rms} > 0.436\ V$$ **Equation 14.**

The corrected voltages are applied to **Equation 7** and **Equation 8** to obtain the temperature difference values. The time series of thermosonde temperature differences are shown in **Figure 7**. To determine the validity of the thermosonde measurements before calculating C_n^2, the thermosonde temperature differences are compared to the vertical temperature differences measured by the radiosonde. Both the Graw radiosonde and the thermosonde sample at 1 Hz; hence, the temperature differences can easily be temporally matched. The radiosonde vertical temperature difference is found by dividing the difference in temperature between each radiosonde measurement by the difference in altitude between each measurement. The precision of the radiosonde (0.1 K) is much lower than the thermosonde (0.001 K); therefore, this comparison is meant to confirm that the temperature differences measured by the thermosonde are generally comparable to the radiosonde temperature differences. After an initial temperature difference increase shortly after launch, the radiosonde recorded negative temperature differences through the troposphere. A very large increase in thermosonde temperature differences is located at almost the same time as the radiosonde temperature difference; therefore, the large increase is likely caused by an inversion. At approximately 21,900 seconds, the radiosonde reports positive temperature differences, which indicates the package crossing the tropopause and entering the stratosphere. Before the package reaches the stratosphere, the thermosonde temperature differences exhibit an increasing number of large increases that quickly stop after the package reaches the stratosphere. The mean thermosonde temperature difference value also decreases after the radiosonde begins recording positive vertical temperature difference values, which suggests that the thermosonde is resolving the turbulence around the tropopause. The absolute values of the radiosonde vertical temperature differences shown a more direct comparison of the range of differences measured by both the radiosonde and thermosonde. Aside from the time window between the two major increases in thermosonde temperature differences, the radiosonde temperature differences match up well with the thermosonde temperature differences. The radiosonde temperature differences do not exhibit the increase that the thermosonde temperature differences exhibit due to the lower precision of the radiosonde's temperature sensor, but the radiosonde values roughly agree with the average thermosonde values.

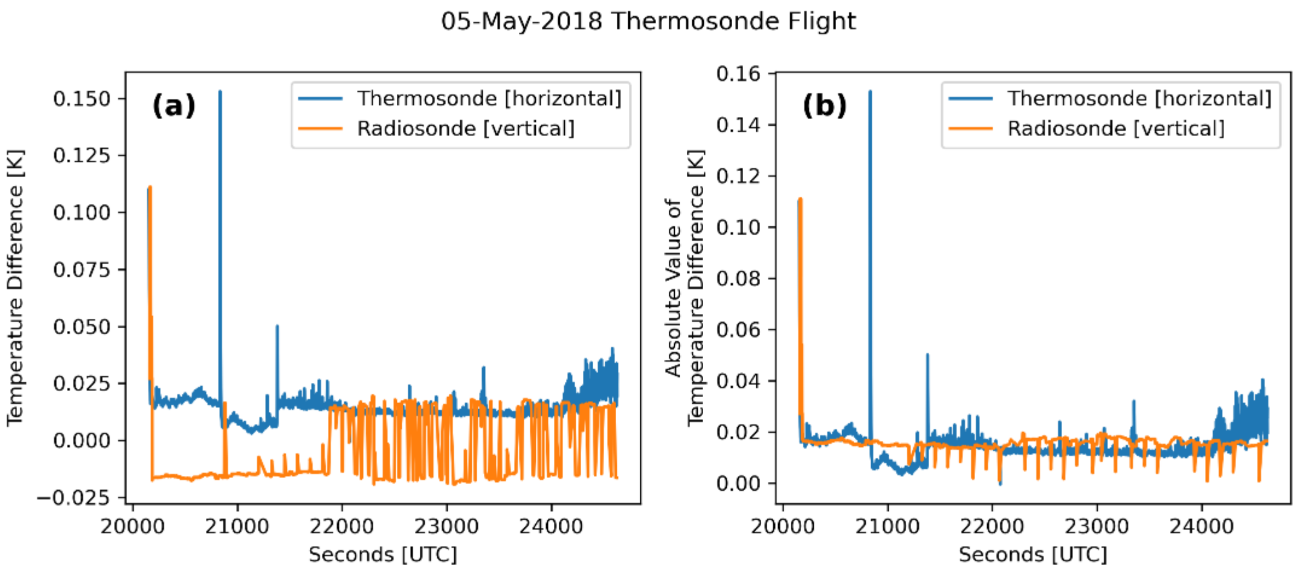

Figure 7. Comparison of the 1-m horizontal temperature differences observed by the thermosonde (blue) with the 1-m vertical temperature differences derived from the radiosonde data (a, orange) and the absolute value of the radiosonde vertical temperature differences (b, orange) from the 05Z 5 May 2018 thermosonde launch.

The 05Z 05 May 2018 HRRR model sounding (**Figure 8a**, red) agrees very well with the radiosonde profile (**Figure 8a**, blue) observed during the flight. The radiosonde and model soundings show a strong temperature inversion at 950 mb. A small temperature inversion is present at approximately 550 mb (~4900 m), and the peak wind speed of 60 kts is near 300 mb. **Figure 8b** is the temperature difference profile from the thermosonde during the 5 May 2018 launch. The temperature differences in the lower 4.5 km are approximately 0.02 K, with slight variations. At approximately 5 km, there is a large increase up to 0.15 K, and after the increase the temperature differences drop to half of the pre-increase value. The same level of variability before the increase is apparent after the increase. At 9.5 km, there is another large increase, and the temperature differences increase back to around 0.02 K. The increase near the surface is a valid measurement; however, the two large positive increases are likely artifacts due to the data logging software. At approximately 13 km, there is a temperature difference that drops below 0 K, which is also likely an artifact. Both the model and radiosonde estimates show C_n^2 values between 10^{-14} and 10^{-15} $m^{-2/3}$ in the lowest 2 km of the atmosphere, with a very sharp decrease in C_n^2 at about 3 km down to C_n^2 on the order of 10^{-17} and 10^{-16} (**Figure 8c**). Due to the differences in resolution between the radiosonde data and model sounding, the radiosonde-estimated ${C_n}^2$ exhibits much more variability than the HRRR model sounding. The radiosonde profile is averaged to match the resolution of the radiosonde data to that of the model sounding, which enables a direct comparison of the datasets, following the methodology of Frehlich et al.[11] The radiosonde data (temperature, pressure, and u and v-wind components) are averaged around each HRRR model altitude so the vertical resolution of the radiosonde data is consistent with the HRRR profile's vertical resolution. The average of the differences of the profiles' logarithmic C_n^2 estimations is 0.005 +/- 0.159. For the troposphere, the average difference is 0.017 +/- 0.183; for the stratosphere 0.024 +/- 0.073.

The temperature differences are matched to the radiosonde data using the thermosonde timestamp, and the Dale-Gladstone Relation (**Equation 12**) applied to the combined data to obtain C_n^2. The thermosonde C_n^2 and radiosonde-estimated C_n^2 (**Figure 8c**) show many of the features seen in the thermosonde temperature differences (**Figure 8b**), including the increase in thermosonde C_n^2 just below the tropopause (approximately 12 km). A comparison of the thermosonde C_n^2 after averaging to match the resolution of the averaged radiosonde-estimated C_n^2 is seen in **Figure 8**c. The averaging removes several features apparent in **Figure 8b**, including the increasing thermosonde values near the tropopause. For the 05 May 2018 flight, the average logarithmic C_n^2 difference between the thermosonde and radiosonde-estimated C_n^2 is 0.260 +/- 0.535. For the troposphere, the average difference is 0.058 +/- 0.628; for the stratosphere, the average difference is 0.410 +/- 0.441. For comparison, Frehlich et al. found an average difference value of 0.065 +/- 1.236 for the troposphere and an average difference value of 0.116 +/- 0.359 for the stratosphere.[11]

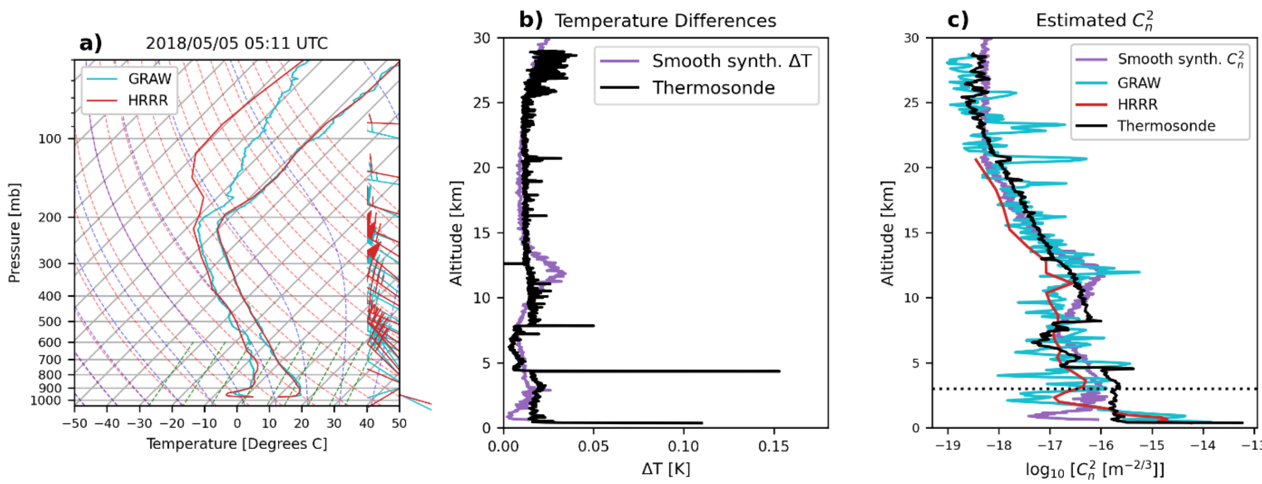

Figure 8. Data from the 05 May 2018 thermosonde launch starting at 05:11 UTC from the Glacial Ridge Observatory near Mentor, MN. a) Skew-T Log-P diagram of the Graw DFM-09 radiosonde (cyan) and the High-Resolution Rapid Refresh (HRRR) model sounding for the time and location of the launch (red). b) Thermosonde-measured (black) and smooth synthetic (purple) temperature differences. c) thermosonde-calculated (black), radiosonde-estimated (cyan), smooth synthetic (purple), and model-estimated (red) C_n^2. The dotted line represents the 3 km minimum for evaluating the error between the profiles. Synthetic temperature differences and ${C_n}^2$ data are derived from the monthly climatology of Bismarck 12Z radiosonde data.

Plotting the C_n^2 and ΔT for the 05 May 2018 thermosonde flight with the synthetic C_n^2 and ΔT derived from the KBIS 12Z May 2018 sounding climatology allows for general comparisons between the measured and synthetic values (**Figure 8**b and c, purple). A similar increase in ΔT and C_n^2 near the tropopause level seen in the thermosonde measurements is found in the synthetic profiles (**Figure 8b** and **Figure 8c**, respectively). The general profile of the synthetic C_n^2 follows a similar path of the measured C_n^2 profile, with surface values on the order of 10^{-14} that decrease to 10^{-16} just below the tropopause, where the profile increases above 10^{-16}. Above the tropopause, the profiles decrease from 10^{-16} to 10^{-18} at 20 km. The synthetic ΔT also parallels the measured ΔT profile, although the synthetic ΔT profile reports higher values near the tropopause than those reported by the measured ΔT profile.

C) 4 May 2019 Balloon Flight

A second balloon flight was conducted on 04 May 2019 at 03:00 UTC, with the launch site moved to Mayville State University in Mayville, ND. One of the main goals of the second launch is to determine if changes to the thermosonde's electronic components allow for more variability in the voltage measurements than in the 5 May 2018 launch. As with the 5 May 2018 first launch, the raw temperature difference is adjusted through the noise floor correction (**Figure 9a**) and the temperature difference conversion (**Figure 9b**). The resulting temperature difference values, as well as the meteorological variables from the radiosonde, are used to calculate C_n^2.

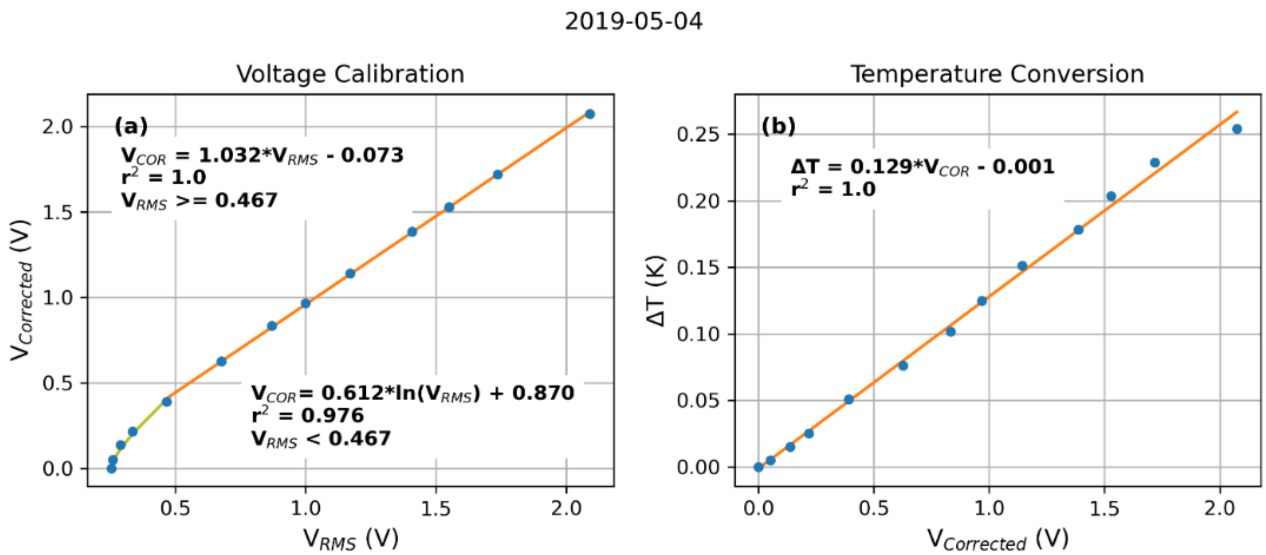

Figure 9. a) Voltage correction relations for the thermosonde data from the second thermosonde flight at 03:00 UTC 04 May 2019. b) Conversion relation between the corrected voltages and the temperature difference values.

Due to an unexpected early loss of communication with the thermosonde during the 4 May 2019 flight, data are only available for approximately the first half of the thermosonde ascent, from the surface to an altitude of approximately 6.5 km. The radiosonde and HRRR model profiles (**Figure 10a**) show general agreement from the surface until the loss of radiosonde data. The HRRR profile correctly resolves the surface inversion; however, it does not resolve the capping inversion at the top of the residual boundary layer at approximately 750 mb. C_n^2 profiles estimated from the averaged radiosonde data (**Figure 10c**, blue) and the HRRR model sounding (**Figure 10c**, red) show ${C_n}^2$ values between 10^{-15} and 10^{-14} $m^{-2/3}$ near the surface, with a very sharp decrease in C_n^2 just above the surface to about 10^{-16} $m^{-2/3}$. Due to the differences in resolution between the radiosonde data and model sounding, the radiosonde-estimated ${C_n}^2$ exhibits much more variability than the HRRR model sounding. The radiosonde-estimated C_n^2 vary by several orders of magnitude between 1 km and 6 km, while the HRRR values only vary within a single order of magnitude. Due to the early termination of the radiosonde, there is limited data to calculate the comparison statistics for the profiles above 3 km. As with the 5 May 2018 flight, thermosonde C_n^2 are calculated from the temperature differences and the radiosonde meteorological measurements. As shown in **Figure 10c**, both the radiosonde-estimated C_n^2 and the thermosonde C_n^2 exhibit variability during the ascent, with the radiosonde estimates showing larger amplitude variations than the thermosonde values. The thermosonde C_n^2 values are approximately two orders of magnitude larger than the radiosonde-estimated values at the surface, but above 1 km, both profiles oscillate around values on the order of $10^{-16.5}$. The profile stops at just over 6 km due to lost connection; therefore, the C_n^2 behavior in the upper atmosphere near the tropopause is not quantifiable. However, from the 6 km of data the thermosonde collected, strong variability in both the radiosonde-estimated and thermosonde C_n^2 is seen.

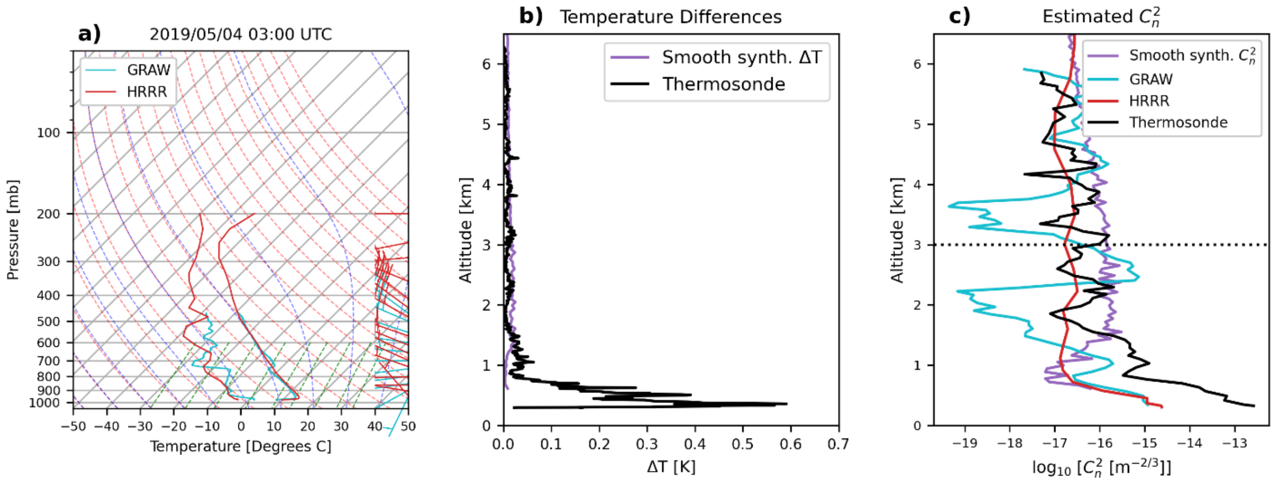

Figure 10. Data from the thermosonde launch on 04 May 2019 at 03:00 UTC from the Mayville State University campus in Mayville, ND. a) Skew-T Log-P diagram of the Graw DFM-09 radiosonde in the thermosonde instrument package (blue) and the High-Resolution Rapid Refresh (HRRR) model sounding for the time and location of the launch (red). b) Thermosonde-measured temperature differences. c) thermosonde-calculated (black), radiosonde-estimated (blue), and model-estimated (red) C_n^2. The dashed line represents the 3 km minimum for evaluating the error between the profiles. Synthetic temperature differences and C_n^2 data are derived from the monthly climatology of Bismarck 12Z radiosonde data.

DISCUSSION

The radiosonde-estimated C_n^2 obtained from the 5 May 2018 launch agree with the estimated C_n^2 profile calculated from the HRRR forecast sounding. A surprising similarity between the radiosonde and model estimated C_n^2 is the stark agreement in the sharp decrease in C_n^2 near the 3 km level of the 5 May 2018 launch (**Figure 8c)**. The average logarithmic difference between the radiosonde and model C_n^2 is much smaller than the statistics reported by Friehlich et al;[11] however, the degree that the thermosonde data match the radiosonde data is not as high as anticipated. Previous studies, including Jumper et al.,[16] observed significant variability in C_n^2 data through the entire profile. As seen in **Figure 8**, the general pattern of the thermosonde C_n^2 profile and the radiosonde-estimated C_n^2 profile above 10 km agree, but the amount of variability in the thermosonde data is not as large as that of the smoothed radiosonde C_n^2 profile or of the results found by Frehlich et al. and Jumper et al.[11, 16] Near the 20 km level during the 5 May 2018, there is a large increase in radiosonde-estimated C_n^2 and a smaller increase in thermosonde C_n^2 that agrees with an increase in the radiosonde-estimated C_n^2. Below 10 km, however, there is less similarity between the profiles. Despite the apparent resolution differences between the USIP thermosonde and the thermosondes used in the Frehlich et al. study, as well as the apparent disagreement seen in **Figure 8**, the statistical comparison values from the 5 May 2018 flight thermosonde launch are close to the values reported by Frehlich et al. The average difference in logarithmic C_n^2 in the troposphere found during the 5 May 2018 flight launch is 0.058 +/- 0.628; the corresponding value from the Frehlich et al. study was 0.065 +/- 1.236.[11] The range of values from the full-flight launch is well within the range of values from the Frehlich et al. study. For the stratosphere, the average difference in logarithmic C_n^2 from the full-flight launch is 0.410 +/- 0.441; the corresponding value from the Frehlich et al. study was 0.116 +/- 0.359.[11] The stratospheric difference values are not as comparable as the tropospheric difference; however, the ranges of the two values have a significant overlap that suggests the values seen in the free-flight launch are reasonable.

The comparisons between the measured data from the thermosonde balloon launch and the synthetic data show general agreement between the two datasets. The synthetic C_n^2 and ΔT profiles follow very similar paths to the C_n^2 and ΔT measured during the thermosonde balloon launch. The measured C_n^2 profile closely follows the synthetic profile up to just over 20 km. The synthetic profiles lack the variability seen in the measured profiles, due to the methods used to calculate synthetic values. The area with the most disagreement between the synthetic and measured profiles is near the tropopause in the ΔT profiles. Aside from several increases, the observed thermosonde temperature differences do not deviate far from 0.02 K. Near the tropopause, some of these increases grow larger, but the average values stay around 0.02 K. In the synthetic ΔT, however, the ΔT values increase significantly near the tropopause, with the 11-point averaged ΔT increasing to around 0.04 K; after the tropopause, the values decrease again back to around 0.02 K. One possible source of this large increase is the methods used to calculate the synthetic ΔT values from the synthetic C_n^2 values, and the behavior of the synthetic C_n^2 near the tropopause could be driving the large increase in ΔT at the tropopause. Despite a few differences, the synthetic C_n^2 and ΔT profiles calculated from the May 2018 sounding climatology compare well with the measured C_n^2 and ΔT profiles from the thermosonde balloon launch.

A few surprising results have come out of the 5 May 2018 flight. One large surprise is the lack of large-scale variability in both the raw and smoothed thermosonde data. The thermosonde data collected by Frehlich et al. exhibit much variability from the surface up to 30 km.[11] While the thermosonde data from the first free-flight launch does exhibit some small variability around the average profile, the variability is nowhere near the level of variability seen in the Frehlich et al. paper. This could be due, in part, to slight differences in the make-up of the thermosondes between the USIP project and the project outlined in Frehlich et al. [11] Previous studies involving thermosondes, such as the study by Murphy et al., used 2.5 micron-diameter platinum wires as the thermosonde probes.[12] While the original plan for the USIP project was to use 2.5 micron-diameter platinum wires, 2 micron-diameter platinum wires had to be substituted because of the extreme difficulty in finding 2.5 micron-diameter platinum wires. The same methods for accounting for the resistance differences with the 2.5 micron-diameter wires were applied to the 2 micron-diameter wires, potentially introducing error into the final temperature difference measurements. A possible cause for the lack of variability in the thermosonde data is that the sensitivity of the thermosonde is not as high as planned. The differences in platinum wire sizes could affect the sensitivity of the instrument.

For the 4 May 2019 flight, the thermosonde signal processing components are reworked to increase the sensitivity of the instrument. The vertical variability in the 4 May 2019 flight thermosonde C_n^2 is significantly higher than in the 4 May 2018 flight, although the thermosonde C_n^2 from the second launch does not match as well with the variability in the radiosonde-estimated C_n^2. The increased variability indicates that the changes made to the thermosonde improve the C_n^2 measurements. However, the thermosonde C_n^2 seems to be out of phase with the radiosonde-estimated C_n^2. The exact cause of this out-of-phase relationship is not known. It could be due to problems with the connection between the radiosonde and thermosonde, as features in the radiosonde-estimated profile appear similar to features in the thermosonde profile at lower altitudes.

CONCLUSIONS

A digital thermosonde instrument is developed and built by students from the UND Electrical Engineering department. When comparing the tethered test temperature difference values to the synthetic temperature differences derived from the 00Z November 2017 Bismarck, ND C_n^2 climatology, the true temperature differences are on the low end of what is expected; however, this is reasonable for the stable air. The 5 May 2018 flight of the had thermosonde estimated profiles of C_n^2 from the radiosonde data and a model sounding that agreed very well. While the radiosonde-estimated C_n^2 and the thermosonde C_n^2 do not agree as well, the range of comparison values is consistent with those seen in previous studies. The horizontal temperature differences measured by the thermosonde are close to the vertical temperature differences calculated from the radiosonde data, and significant atmospheric features found in the radiosonde data can also be found in the thermosonde data, which supports the validity of the thermosonde measurements. The observations from the second thermosonde launch conducted on 4 May 2019 showed increased sensitivity to varying optical turbulence through the lower atmosphere.

AVAILABILITY

All data collected during this project, and used to create the figures within this article, are available in a University of North Dakota online data collection.[17] All programs used for data processing, analysis, and visualization are stored online in the open-source Sourceforge repository for the Airborne Data Processing and Analysis (ADPAA) software packages[15], which is archive via Zenodo.[18]

ACKNOWLEDGEMENTS

This research is part of a NASA-funded Undergraduate Student Instrument Project (USIP). Additional thanks go out to the rest of the USIP team. From the UND Space Studies department and the North Dakota Space Grant Consortium, thanks to Dr. James Casler, Dr. Ron Fevig, Dr. Caitlin Milera, Dr. Marissa Saad, and Denise Buckner for organizing the project and planning balloon launches. From the UND Electrical Engineering department, thanks to Dr. Naima Kaabouch, Michael Mullins, and Kyle Foerster for building and maintaining the thermosonde for the many tests and launches.

REFERENCES

1. K. W. Fischer, M. R. Witiw, J. A. Baars, and T. R. Oke, "Atmospheric laser communication," *Bull. Am. Meteorol. Soc.*, vol. 85, no. 5, pp. 725–732, May 2004, doi: 10.1175/BAMS-85-5-725.
2. E. M. Dewan, "Optical Turbulence Forecasting: A Tutorial," AIR FORCE GEOPHYSICS LAB HANSCOM AFB MA, AFGL-TR-80-0030, Jan. 1980. Accessed: Mar. 15, 2019. [Online]. Available: https://apps.dtic.mil/docs/citations/ADA086863
3. V. I. Tatarski, *Wave Propogation in a Turbulent Medium*. New York, NY: McGraw-Hill Book Company, Inc., 1961.
4. A. M. Obukhov, "On the Distribution of Energy in the Spectrum of Turbulent Flow," *Dokl. Akad Nauk SSSR*, vol. 32, no. 4, 1941.

5. A. N. Kolmogorov, "Dissipation of Energy in Locally Isotropic Turbulence.," *Dokl. Akad Nauk SSSR*, vol. 32, 1941.
6. J. L. Bufton, "A RADIOSONDE THERMAL SENSOR TECHNIQUE FOR MEASUREMENT OF ATMOSPHERIC TURBULENCE," Goddard Space Flight Center, Greenbelt, Maryland, Technical Note, 1975. [Online]. Available: https://ntrs.nasa.gov/archive/nasa/casi.ntrs.nasa.gov/19750008971.pdf
7. E. M. Dewan, R. E. Good, R. Beland, and J. Brown, "A Model for Csubn(2) (Optical Turbulence) Profiles Using Radiosonde Data," PHILLIPS LAB HANSCOM AFB MA, PL-TR-93-2043, Mar. 1993. Accessed: Mar. 15, 2019. [Online]. Available: https://apps.dtic.mil/docs/citations/ADA279399
8. R. E. Hufnagel, "Propagation Through Atmospheric Turbulence," in *The Infrared Handbook, Ch. 6*, 1978.
9. T. E. Van Zandt, K. S. Gage, and J. M. Warnock, "An Improved Model for the Calculation of Profiles of CN2 and e in the Free Atmosphere from Background Profiles of Wind, Temperature, and Humidity.," presented at the 20th Conference on Radar Meteorology, American Meteorological Society, Boston, MA, 1979.
10. D. J. Richardson, "Solar heating effects on balloon-borne microthermal probes for the airborne laser program," Master's Thesis, Naval Postgraduate School, Monterey, CA, 1997. [Online]. Available: https://calhoun.nps.edu/bitstream/handle/10945/8977/solarheatingeffe00rich.pdf?sequence=1
11. R. Frehlich *et al.*, "Estimates of Cn2 from Numerical Weather Prediction Model Output and Comparison with Thermosonde Data," *J. Appl. Meteorol. Climatol.*, vol. 49, no. 8, pp. 1742–1755, Apr. 2010, doi: 10.1175/2010JAMC2350.1.
12. E. Murphy, P. Tracy, R. Beland, G. Jumper, K. Robinson, and G. Clement, "THERMOSONDE 2007: In-Situ Measurement of Optical Turbulence," Air Force Research Laboratory, Scientific, Final, May 2007. [Online]. Available: https://apps.dtic.mil/dtic/tr/fulltext/u2/a551490.pdf
13. J. Wendell, A. F. Jordan, "iMet-1-RSB Radiosonde XDATA Protocol & Daisy Chaining," *National Oceanic and Atmospheric Administration technical document*. Jan. 2016. [Online]. Available: https://gml.noaa.gov/aftp/user/jordan/iMet-1-RSB%20Radiosonde%20XDATA%20Daisy%20Chaining.pdf
14. A. Krauchi, R. Philipona, G. Romanens, D. F. Hurst, E. G. Hall, and A. F. Jordan, "Controlled weather balloon ascents and descents for atmospheric research and climate monitoring," *Atmospheric Meas. Tech.*, vol. 9, no. 3, pp. 929–938, Mar. 2016, doi: 10.5194/amt-9-929-2016.
15. D. J. Delene, "Airborne data processing and analysis software package," *Earth Sci. Inform.*, vol. 4, no. 1, pp. 29–44, Mar. 2011, doi: 10.1007/s12145-010-0061-4.
16. G. Jumper, J. Vernin, M. Azout, and H. Trinquet, "Comparison of Recent Measurements of Atmospheric Optical Turbulence," in *36th AIAA Plasmadynamics and Lasers Conference*, Toronto, Ontario, Canada, Jun. 2005. doi: 10.2514/6.2005-4778.
17. B. T. Sorenson and D. J. Delene. "Data in 'Development at the University of North Dakota of a Digital Thermosonde Instrument for the Study of Atmospheric Optical Turbulence (C_n^2)'", Dec. 2023. *Datasets*. 29. doi**:** https://doi.org/10.31356/data029. Available: https://commons.und.edu/data/29.
18. Delene, David J., A. Skow, J. O'Brien, N. Gapp, S. Wagner, K. Hibert, K. Sand, and G. Sova, Airborne Data Processing and Analysis Software Package (Version 4267), Zenodo, 22 June 2022, doi:10.5281/zenodo.6685679.

ABOUT STUDENT AUTHORS

Blake Sorenson received a B.S. in Atmospheric Sciences from the University of North Dakota in 2018. He is currently a Ph.D. student in the Atmospheric Sciences program at the University of North Dakota, where he is using remotely-sensed satellite observations to study the radiative impacts of biomass burning aerosols on the Arctic climate and on Arctic sea ice.

PRESS SUMMARY

A NASA Undergraduate Student Instrument Project is building a digital thermosonde instrument to study atmospheric optical turbulence, which is the distortion of light waves by temperature changes in the atmosphere. Optical turbulence makes images of Earth taken from satellites appear wavy and unclear, as well as negatively affecting laser signals moving up through the atmosphere into space. The thermosonde is flown on a high-altitude weather balloon and collects very high-resolution differences in temperature between two fine-wire platinum probes.

Appendix A: Monthly Climatology of Radiosonde-Estimated Atmospheric Optical Turbulence (${C_n}^2$)

*Blake Sorenson[*a], David Delene[a]*

[a]Department of Atmospheric Sciences, University of North Dakota, Grand Forks, ND

Mentors: David Delene, Atmospheric Sciences

Many previous studies of atmospheric optical turbulence have been conducted using balloon-borne thermosonde instruments and high-resolution numerical weather prediction model simulations.[1-3] However, A review of the literature does not reveal any previous work in developing a climatology of averaged refractive index structure parameter profiles (${C_n}^2$) for the atmosphere above National Weather Service offices. Knowing the range of ${C_n}^2$ in each atmospheric layer over a certain location could provide a rough estimate of the optical turbulence over a given area without needing to fly thermosondes or use other expensive means to obtain high-resolution ${C_n}^2$ data.

For the NASA USIP thermosonde project at the University of North Dakota, a monthly climatology of ${C_n}^2$ for 2017 is developed to determine the range of ${C_n}^2$ values could be expected from thermosonde launches. The AFGL model for estimating ${C_n}^2$ from radiosonde data, given by

$$ {C_n}^2 = 2.8[(\frac{79\times10^{-6}P}{T^2})(\frac{\partial T}{\partial z}+\gamma)]^2(0.1)^{4/3}10^{Y(z)}, \qquad \textbf{Equation 1.} $$

where

$$ Y(z) = 1.64 + 42.0 \times S_{raw} \text{ (Troposphere)} \qquad \textbf{Equation 2.} $$

$$ Y(z) = 0.506 + 50.0 \times S_{raw} \text{(Stratosphere)} \qquad \textbf{Equation 3.} $$

and

$$ S_{raw} = \sqrt{\frac{\partial u}{\partial z}^2 + \frac{\partial v}{\partial z}^2} \qquad \textbf{Equation 4.} $$

where P is atmospheric pressure in mb, T is temperature in Kelvin, and γ is the dry adiabatic lapse rate,[4] is utilized to estimate ${C_n}^2$ profiles for each NWS sounding in each month of the year, and the data in each profile between each standard pressure level of the atmosphere are averaged. This results in a set of 30 or 31 averaged logarithmic ${C_n}^2$ values between each major atmospheric pressure level, from the surface to 925 mb, 925 mb to 850 mb, 850 mb to 700 mb, etc. The average and standard deviation of the averaged ${C_n}^2$ data in each layer are calculated, resulting in an average and standard deviation of logarithmic ${C_n}^2$ for each layer for that month. A climatology of refractive index structure parameter profiles for Bismarck, ND for each month of 2017 is compiled from 00Z and 12Z soundings launched at the Bismarck National Weather Service office.

Figure 11a is the climatology of ${C_n}^2$ for 12Z May 2017 at Bismarck. Several features of note can be seen in the climatology. The ${C_n}^2$ values are higher in the lowest few layers of the atmosphere, corresponding to the higher temperatures and wind shear in that part of the atmosphere. The highest ${C_n}^2$ standard deviations are mostly found in the lowest few layers of the atmosphere, and this is due largely to the fact that the lower atmosphere changes temperature and wind speed much more than the upper atmosphere. The ${C_n}^2$ values decrease steadily from the surface to the 400 – 300 mb layer. A local maximum in average ${C_n}^2$ is found in the 300 mb to 200 mb layer, corresponding to the average height of the tropopause; this increase in optical turbulence is expected near the tropopause.[1] Above this local maximum of ${C_n}^2$, the boxplots decrease significantly through the highest layer.

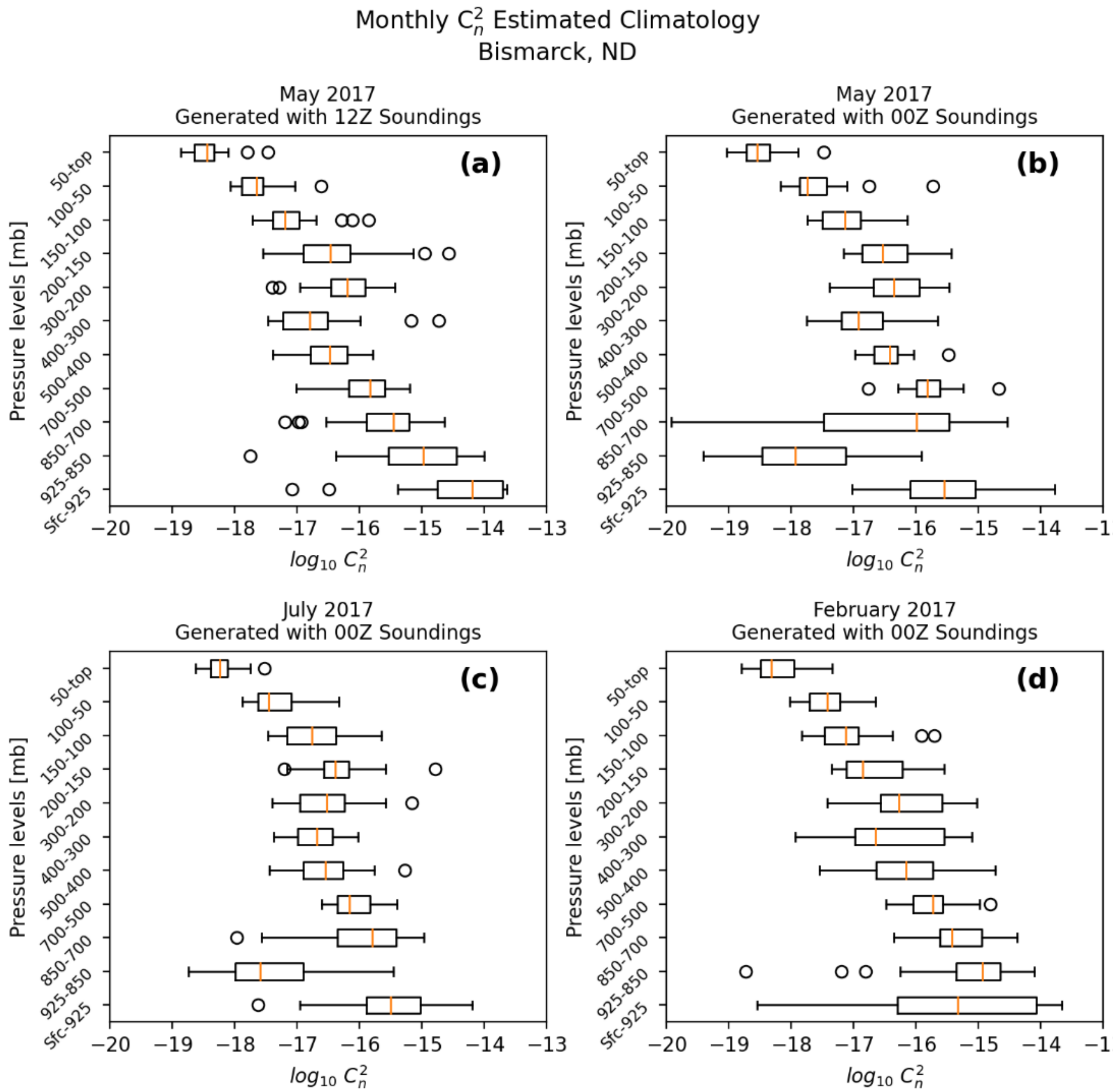

Figure 11. A climatology of refractive index structure parameter profiles estimated from Bismarck, ND National Weather Service radiosonde profiles consisting of (a) 12Z soundings from May, 2017; (b) 00Z soundings from May, 2017; (c) 00Z soundings from July, 2017; (d) 00Z soundings from February, 2017

Several interesting patterns emerge when comparing the 12Z May 2017 Bismarck, ND ${C_n}^2$ climatology to the 00Z May 2017 Bismarck climatology, shown in **Figure 11b**. While the data in the lower three layers of the 12Z May climatology decrease almost linearly, the data in the lower three layers of the 0Z May climatology are about two orders of magnitude smaller than the data in the layers above and below it. The large differences in ${C_n}^2$ between the lower three layers in the May climatology are indicative of the taller late-spring boundary layer. One possible cause for this difference could be that the thermal and kinematic properties of the upper boundary layer are causing the AFGL model to put much lower values of ${C_n}^2$ in that region. Static stability could also be playing a role here. In the spring, the 12Z soundings from Bismarck are usually very stable from radiational cooling overnight, while the 00Z soundings are usually well mixed to about the 850 millibar level. Since Bufton showed that higher values of ${C_n}^2$ are found near the tropopause,[6] which is an area of high static stability, it could be that lower atmospheric layers with high static stability also exhibit higher ${C_n}^2$ while layers with lower static stability exhibit lower ${C_n}^2$.

A pattern like the changes in upper-boundary-layer ${C_n}^2$ can be seen when comparing summer 00Z profiles to winter 00Z profiles. **Figure 11c** and **Figure 11d** show the Bismarck 00Z July 2017 and Bismarck 00Z February 2017 ${C_n}^2$ climatologies, respectively. The two main features that differ between these two climatologies are the upper-boundary-layer ${C_n}^2$ values and the tropopause height. As previously discussed, higher values of ${C_n}^2$ are generally seen near the tropopause. In February, since the air in Bismarck, ND is much colder than it is in July, the tropopause is lower than it is in July. The tropopause-induced ${C_n}^2$ maxima in the February climatology is found in the 300 mb to 200 mb level; in the July climatology that ${C_n}^2$ maximum is found in the layer above, which is the 200 mb to 150 mb level. The second, and more pronounced, difference between the two seasonal ${C_n}^2$ profiles is the drastic difference in ${C_n}^2$ in the upper boundary layer. The lower atmosphere in February in Bismarck, ND is much more statically stable than the lower atmosphere in July in Bismarck. Hence, the ${C_n}^2$ values in the 925 mb to 850 mb level in the 00Z February 2017 Bismarck ${C_n}^2$ climatology are, on average, three orders of magnitude larger than in the 00Z February 2017 Bismarck ${C_n}^2$ climatology.